INDEX COPERNICUS INTERNATIONAL



Bio-Algorithms and Med-Systems

WWW.BAMSJOURNAL.COM ISSN: 1896-530X

ORIGINAL ARTICLE

Received: 12.08.2024
Accepted: 28.10.2024
Published: 27.12.2024

CITE THIS ARTICLE AS:
Das P, Verma R, Prasad K, "Exploring PET imaging with scattered photons and polarization characteristics," Bio-Algorithms and Med-Systems vol. 20, special issue, pp. 101-110, 2024, DOI: 10.5604/01.3001.0054.8576

AUTHORS' CONTRIBUTION:
A. Conceptualization
B. Data Curation
C. Formal Analysis
D. Funding Acquisition
E. Investigation
F. Methodology
G. Project Administration
H. Resources
I. Software
J. Supervision
K. Validation
L. Visualization
M. Writing – Original Draft
N. Writing – Review & Editing

CORRESPONDING AUTHOR:
Pragya Das; Indian Institute of Technology Bombay, India; E-mail: pragya@phy.iitb.ac.in

COPYRIGHT:
Some rights reserved: Jagiellonian University Medical College. Published by Index Copernicus Sp. z o. o.

OPEN ACCESS:
The content of the journal „Bio-Algorithms and Med-Systems" is circulated on the basis of the Open Access which means free and limitless access to scientific data.

CREATIVE COMMONS CC BY:
Attribution. It is free to copy, distribute, present and perform the copyrighted work and derivative works developed from it, provided that the name of the original author is cited.

Exploring PET imaging with scattered photons and polarization characteristics

Pragya Das[1AEFHJKMN], **Ritesh Verma**[1BCEFIKL], **Kaustav Prasad**[1BCEFIKL]

[1]Indian Institute of Technology Bombay, India

ABSTRACT

Objective: To demonstrate the potential of PET imaging using scattered photons, we have proposed a novel technique that utilizes single-tissue-scattered events based solely on time-of-flight (TOF) information, without relying on energy data. Additionally, we explored the possibility of improving image quality by applying polarization selection criteria for true events.

Methods: Due to Compton scattering within the phantom, scattered photons exhibit reduced energy, which remains unknown in our analysis. For a fixed scattering angle, the locus of the scattering point forms an arc of a circle in two dimensions (2D). With known TOF, we can trace the locus of the annihilation point for all possible scattering angles and positions. Our procedure involves identifying the annihilation-point loci corresponding to all pairs of single-scattered photons and merging them. In a separate study, we utilized the classical concept of orthogonal polarization of two annihilation photons, combined with energy filtering, to select genuine (true) events.

Results: Our proof-of-concept study successfully demonstrated that the TOF-based approach could yield an image of a point source. The merging of annihilation-point loci from numerous pairs of single-scattered photons produced a localized region for the source activity. The intensity profile showed a finite width of 14 mm for 1 ps uncertainty in TOF. Additionally, another analysis utilizing polarization and energy criteria generated a clean dataset for true events, with minimal background interference (containing random coincidences) at a high event rate.

Conclusions: The simulation-based study validated our proposed model, indicating its potential to enhance the sensitivity and accuracy of event selection in PET imaging. These findings lay a solid foundation for further research into advanced PET imaging techniques that incorporate single-scattered events.

KEYWORDS

positron emission tomography, compton scattering, time of flight, polarization

LIST OF ABBREVIATIONS

2D – two dimensions
CNR – contrast-to-noise ratio
CoV – coefficient of variation
CRC – contrast recovery coefficient
FWHM – full width at half maximum
GATE – Geant4 Application for Tomographic Emission
J-PET – Jagiellonian positron emission tomography
LOR – Line of Response
MLEM – maximum likelihood expectation maximisation
PET – positron emission tomography
TOF – time-of-flight
WGI – whole gamma imaging

INTRODUCTION

PET research strives to find ways to improve the image quality, but the scattering of photons remains a significant obstacle. Typically, the scattering within the phantom is considered noise and discarded. However, it is often beneficial to incorporate scattered events in PET image reconstruction, especially when true coincidences are low and the scatter fraction is high [1, 2]. There is limited research on using scattered data in PET imaging. Two notable approaches are proposed by Conti et al. [3] and Hemmati et al. [4]. The former suggests using two independent back-projectors for image reconstruction: one for true-coincidence (unscattered) data and another for single-scattered data using TOF-broken-LOR [3]. On the other hand, the latter work [4] presents a mathematical model for determining the position of source activity and the most likely single-scattering point for each scattered event.

In a previous study [5], we introduced an imaging technique that utilizes single scattered events in tissue (phantom) using a Compton--PET system [6–8]. The loci of single scattered points lie on the symmetrical geometrical surfaces [3–5] – prolate spheroid or spindle toroid for the acute or obtuse scattering angles, respectively. We considered only the single scattering in our study, avoiding multiple scattering. We generated the direct images of the source activity distribution by estimating the intersection points of the tissue--scattered surface and the Compton cone of the extra gamma-ray (1157 keV) from a unpure beta-emitter ^{44}Sc [9]. For comparison, we independently obtained images using the usual true triple-gamma coincidences. In a practical situation of low activity distribution, having two independent images – one from the scattered data and another from the true (unscattered) data – could improve sensitivity and provide a better diagnosis. The WGI imaging concept [6] emphasizes using all types of data independently.

In another work [10], we created images from single-scattered data and utilized them as an initial estimate in MLEM image reconstruction. Our work aimed to improve the image quality in the low-count PET scans. Initially, we used both energy and TOF information from the list-mode data to estimate the activity distribution for a Jaszczak-type object using the Lucy-Richardson iterative deconvolution technique. The tissue-single-scattered events were generated using GATE [11]. The deconvoluted images were then used as an initial estimate for the non-TOF-MLEM reconstruction, with the true events using STIR software [12]. Our approach resulted in a significant improvement in the balance between the contrast recovery coefficient (CRC) and coefficient of variation (CoV), compared to other less computational methods of creating initial estimates, such as a uniform estimate. Our findings indicated a notable enhancement in CNR values for all hot rods by stopping at the minimum-squared-error iteration.

Currently, our research focuses on studying image reconstruction using single-tissue-scattered photons detected in PET systems, such as J-PET [13–15], with precise time-of-flight (TOF) information. The aim is to develop a mathematical model and suitable algorithms for image reconstruction. Without the energy information of the scattered photon, determining the locus of the scattering point becomes challenging. However, with the TOF information, we could trace the locus of the annihilation point in a 2-D model. We have successfully identified a region containing the annihilation point by analyzing only the single-tissue-scattered events. It is worth noting that the geometrical picture is broad enough to encompass true (unscattered) events as well, as if they occur with a scattering angle of zero. We are also expanding our research to generalize the model to 3-D and applying appropriate filters to enhance the image. The 2-D model and the proof-of--concept study presented here are used to determine the location of a point-source activity using the TOF of single-scattered photons.

The second independent research presented here is a simulation--based study. In this study, we utilized the classical electromagnetic wave nature of photons. Within this framework, the orthogonal polarization of two annihilation photons serves as a selection criterion for genuine (unscattered) events. In our initial investigation, we observed an enhancement in image quality for a low activity distribution when using energy plus polarization binning, compared to the results obtained with only energy binning.

MATERIALS AND METHODS

Tracing annihilation-point locus using single-scattered photons with TOF information

Within a two-dimensional (2-D) framework, the Compton scattering point within the phantom, and an associated geometrical symmetry of its locus, is the key ingredient to our model. As described in the literature [3–5], the locus forms an arc of a circle for a fixed scattering angle (θs). In our earlier work [5], we could determine θs from the measured energy of the scattered photon.

However, in the present work we only rely on accurate information about the time of flight (TOF). This is applicable to a PET system with excellent detector timing resolution, such as the plastic detectors used in J-PET [13–15]. Our work focused on utilizing events corresponding to single scattering within the phantom, while avoiding multiple scattering. The single scattering here means only one of the annihilation photons is scattered at C (Fig. 1.) and detected at B, while the partner photon remains unscattered and is detected at A. The path ACB (= AC + CB) is also called the broken line of response (broken-LOR) [3, 10].

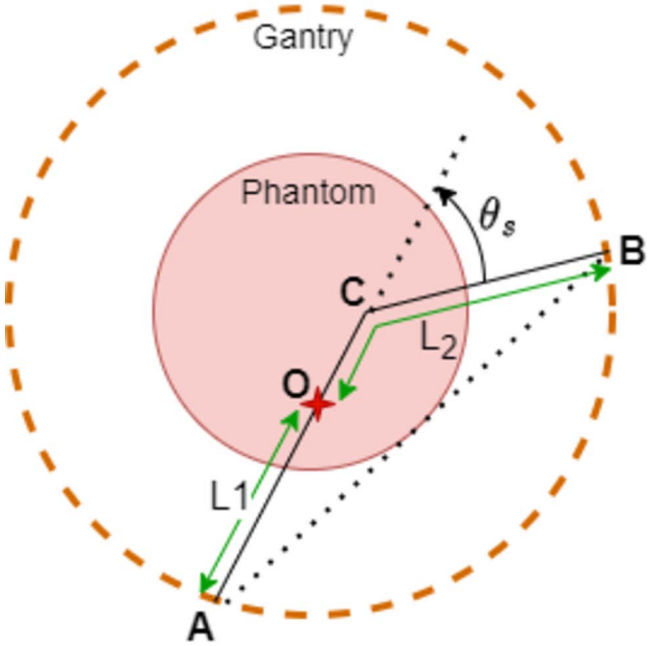

Fig. 1. A pair of annihilation photons originating from the source point O—the unscattered photon is detected at A; the scattering of the other photon happens at C with angle θs and is detected at B. The path lengths of the photons are L_1 and L_2.

Consider a pair of annihilation photons originating from source point O in Fig. 1. On the side AC, the unscattered photon travels a straight path OA (≡*L*1) and the scattered photon takes a broken path (OC + CB ≡L_2) due to scattering at C. Notably, the annihilation point could lie on the side BC as well, implying the detector B detects an unscattered photon and A detects a scattered one. We have considered both possibilities in our analysis. The time of arrival of photons at the detectors A and B are recorded in the list-mode data, from which the time difference (Dt) is extracted, and so is the path length difference ($|L_1 - L_2|$ = c.Dt). Here, c is the velocity of the photon in the phantom medium. To find the values of L_1 and L_2 individually, the total path length $L_1 + L_2$ (≡L = AC + BC) needs to be determined.

There is a clear sight of the annihilation region through broken LOR due to a symmetrical locus of scattering point. Fig. 2. depicts the novelty of our approach based on a simple geometrical construction. The straight line joining the points A and B is the minimum distance (*Lm*) between them. Consider two circles drawn at A and B – with radius r larger than minimum, i.e., r > *Lm* /2 (Fig. 2A.) – intersecting at two points, as shown in red and green dots in the figure. Centred at these two points, another two circles drawn with the same radius r pass through points A and B, constituting the loci of the single scattering point. Only one of them passing through the phantom region is presented in Fig. 2. (B; in green). This observation is interesting enough to realize that the radius r and the scattering angle θs are related, and varying r means changing θs, as shown in Fig. 2B. and 2C. for comparison. There is just one unknown variable, r (or θ s), in our mathematical model in 2-D. Finally, with the geometrical picture of the circular locus with three points, A, B, and C on its circumference, one can determine the total path length of AC + BC (≡L) for a particular value of r.

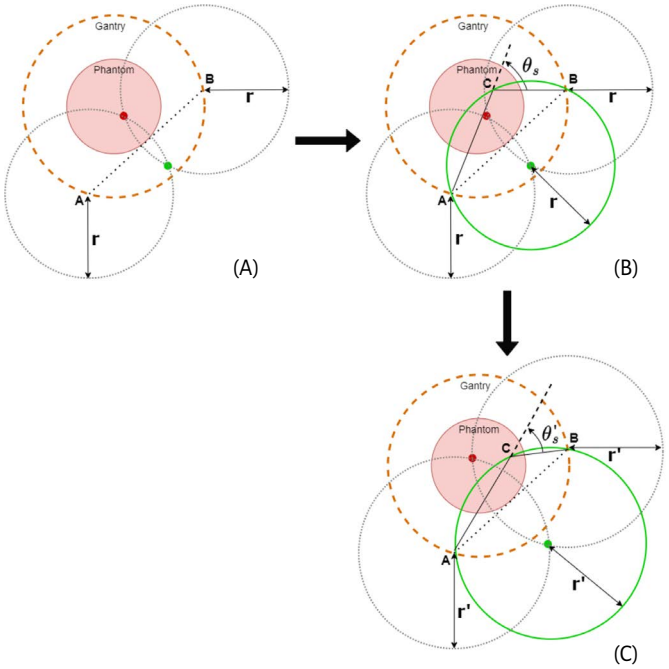

Fig. 2. (A) A geometrical construction by drawing two circles at the detection points A and B first; (B) another circle of the same radius *r* through the intersection point (shown in green) to obtain the locus of the scattering point C; (C) same as part (B) but with a different radius *r'* demonstrating a change in the scattering angle, denoted as θs'.

For the mathematical analysis, we assumed a PET ring of radius 10 cm and a phantom of radius 6 cm in 2-D. To begin, the location of A and B on the ring and the time difference of arrival of photons Dt were somewhat arbitrary. We created many scattering loci as circular arcs by varying θs from 0–900. On each locus, we located many possible scattering points (C) within the phantom region. As discussed earlier, the annihilation point was determined from the knowledge of DL (≡c.Δt) and total path length L. Finally, for each possible C on a particular locus, we obtained a set of annihilation points forming a conic section (locus).

Polarization-directional correlation of annihilation photons

Classically, the wave property of electromagnetic radiation defines the polarization direction (electric vector) in the plane perpendicular to its propagation. The two annihilation photons are emitted in opposite directions and have an orthogonal polarization direction. The use of orthogonal polarization has not been well studied in PET imaging. We corroborated the earlier result [16] of improving the selection of true events with the orthogonal-polarization criterion added to the energy information. Furthermore, we found an overall noise (background) reduction by calculating the peak--to-total intensities.

We utilized GEANT4 (version: 11.1.2) [17] software to generate list--mode data with an event ID, time stamp, detector position, photon energy and polarization. The G4GeneralParticleSource (GPS) is a fundamental component within the GEANT4 toolkit for the Monte-Carlo simulation, with physics lists: G4EmStandardPhysics, G4RadioactiveDecayPhysics, G4DecayPhysics. Further details of the usage of GEANT4 are the particle creation class (G4ParticleGun) producing two photons (back-to-back) of energy 511 keV in a random direction, and setting polarization vectors (SetParticlePolarization [G4ThreeVector]) in a random direction in the plane perpendicular to the photon motion but with 900 offset between the two vectors. We simulated data with Geant4 because the most commonly used software, GATE [11], does not provide the polarization information. A standard-sized PET and water phantom were assumed. The images were reconstructed using the software STIR [12].

RESULTS AND DISCUSSION

PET imaging using single-scattered photons with known TOF

Fig. 3. depicts the loci of annihilation point in pink and cyan dots, for the scattering angle θs = 900, on both possible sides AC or BC (Fig. 1.), assuming DL = 0.1 cm, as an example. Further, by varying the scattering angle we could get the other possible loci within the region bounded by the dots shown in Fig. 3. It produced a region for the location of the source point for one pair of photons detected at A and B. When we extended our analysis to many pairs of photons originating from the same source point, we got the overlapping region of loci and the localized image.

We developed our own C++ codes for creating single-scattered events and implementing our model to estimate the annihilation point. The scattering point is randomly located within the phantom region, and then the detection points are generated based on different scattering angles. The individual path lengths of photons were determined as described earlier. Fig. 4. presents our first result of imaging from 100 pairs of single-scattered photons

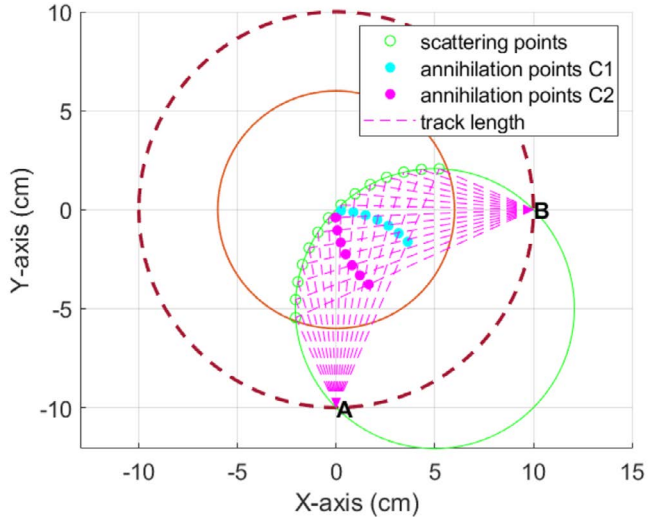

Fig. 3. Loci of annihilation points (pink and cyan dots) for the scattering angle $\theta s = 90°$ for all possible scattering points on its locus (arc in green) within the phantom region, obtained from the geometrical construction explained in the text.

without introducing any error in their detection time. The source point was intentionally off-centered at the location (1,1) to check the accuracy of our model. The image was indeed produced at the source location, but a significant spread was observed even with the precise timing information.

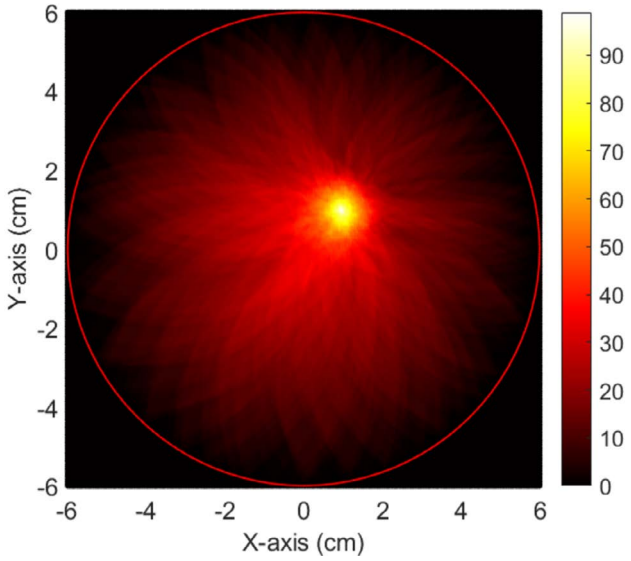

Fig. 4. Estimation of the annihilation point at the location (1, 1) using 100 pairs of single-scattered photons randomly created with precise timing information, by merging locus region for each pair.

We conducted a more extensive investigation with a larger number of events, taking into account uncertainty in the timing information. Fig. 5. displays the results for a centred point source, using 500 pairs of single-scattered events with time uncertainties of (A) 1 ps and (B) 200 ps, and employing Gaussian blurring. The intensity

profiles are also presented. Additionally, Tab. I. compares the FWHM with a result from the literature [5] – the only available result for the single-scattered events based on energy information. The image quality noticeably worsened as the timing uncertainty increased. We expected this due to the underlying geometrical model and its associated uncertainty. Therefore, our proposed idea would work if the timing uncertainty could be minimized.

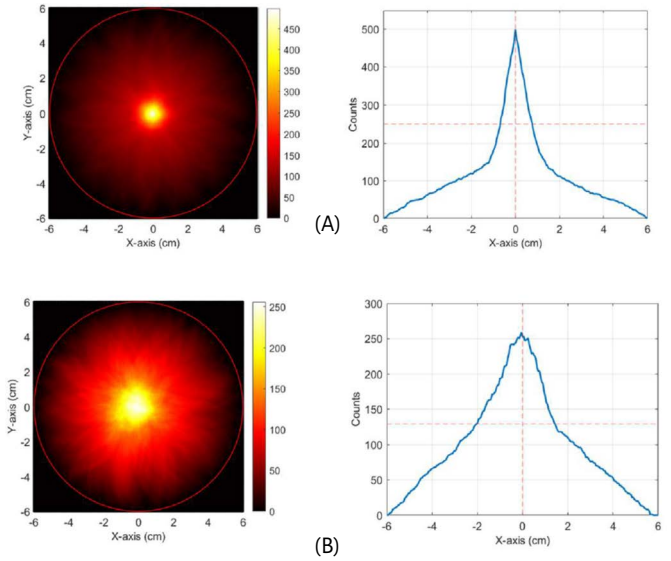

Fig. 5. Images and intensity profiles of a point source at the center of phantom, generated using 500 pairs of single-scattered photons, assuming time uncertainty of (A) 1 ps, and (B) 200 ps.

Tab. I. Comparison of FWHM of the image intensity profiles of a point source created using the tissue-single-scattered events in the (A) present study and (B) an earlier work [5].

TIMING UNCERTAINTY (PS)	(A) FWHM (MM)	(B) FWHM (MM)
1	14	14
200	34	20

As mentioned earlier, the work presented here utilized an in-house computer code to generate only the single-scattered events. Indeed, it was just a proof-of-concept study to validate our model. Later on, we conducted a feasibility study using a realistic data set simulated using the software GATE (version: v9.2). That work was also presented at the conference JS2024, to be published elsewhere. The GATE simulated data contained all events – mainly unscattered (true), single-scattered and multi-scattered – from which we selected the single scattered events for imaging. We also investigated a two-point source. The images were reasonably sharp and well separated after applying a deconvolution technique [10]. We also compared the sensitivity by counting solely the unscattered (true) events with that obtained after combining unscattered and single scattered events. The latter showed significant improvement for the low-activity PET imaging with a high scatter fraction.

Low background and improved image quality with polarization criterion in PET

We attempted PET imaging using multiple types of NEMA activity distributions. There was a consistent observation of a better selection of events with energy plus polarization-based binning compared to only energy-based binning at a high counting rate due to high random coincidences, as discussed in the literature [16]. Fig. 6. compares the sinograms for two activities – 10^8 Bq (top) and 10^9 Bq (bottom) – with energy- (left) and energy-plus--polarization-based (right) selection of events. It is evident from the bottom figure that the overall background is much less in the sinogram on the right than that on the left, illustrating the advantage of event selection using the polarization criterion. We assumed the coincidence time window = 4 ns. We allowed an uncertainty of ±5° for the orthogonal (90°) polarization direction of the two coincident photons, which meant choosing the polarization filtering window between 85°–95°. The energy filtering window was considered for the state-of-art detectors (400–650 keV).

Fig. 7. presents the reconstructed images – with energy binning (left) and energy plus polarization binning (right) – of a water-filled NEMA phantom of total uniform activity of 10^9 Bq. These images show the activity distribution in the circles of radii 1, 2, 3, 4, 6 and 10 mm. The circle of radius 2 mm (marked with an arrow) is crucial to compare in the left and right images, as it appears brighter on the right. The bigger circles seem very similar in intensity, and the 1 mm circle is hardly visible.

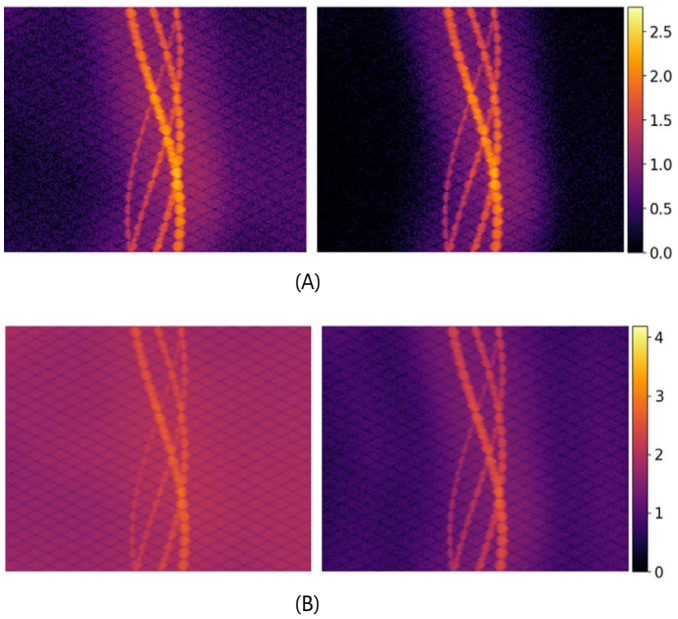

Fig. 6. Comparison of sinograms for two activities, (A) 10^8 Bq and (B) 10^9 Bq, with energy- (left) and energy-plus-polarization (right) based selection of events.

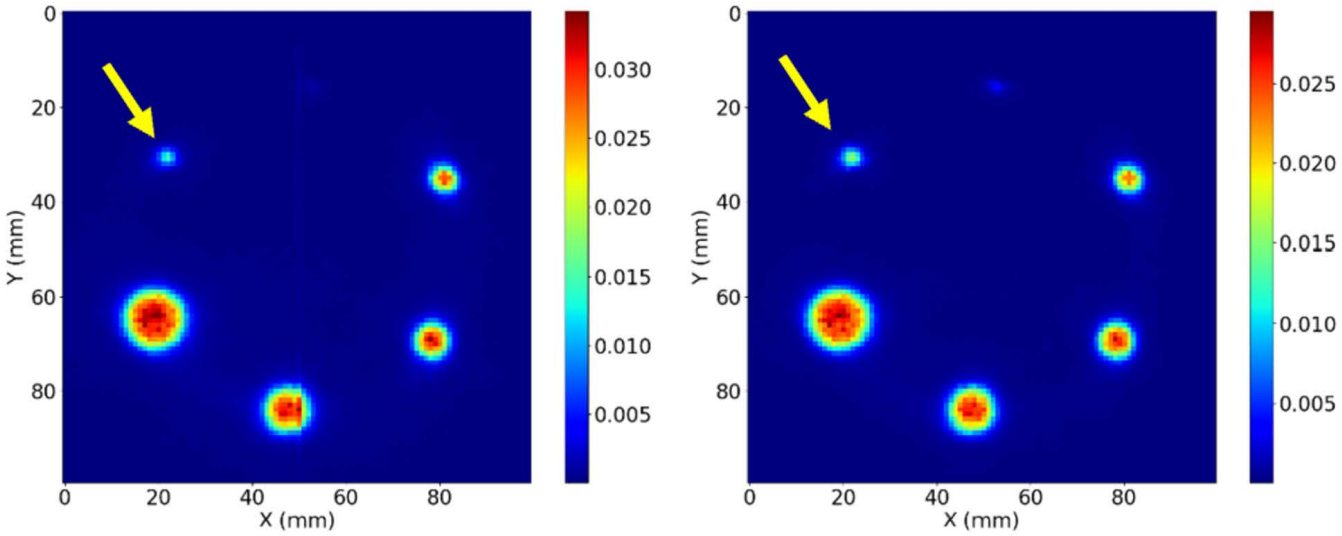

Fig. 7. Reconstructed images based on energy (left) and energy plus polarization (right) selection of the activity distribution in the circles of radii 1, 2, 3, 4, 6 and 10 mm for a water phantom of total uniform activity of 10^9 Bq. The circle of radius 2 mm (marked with an arrow) is brighter in the right figure compared to the left.

The stricter selection using polarization and energy criterion together reduces the counts for each of these circles, as is also apparent from the intensity plot in Fig. 8. This figure is created with a tilted projection (nearly 45°) to obtain a clear separation between the intensity peaks. The peak at the extreme left (marked with an arrow) corresponds to a circle of 2-mm radius. Indeed, this peak (in orange), shows a significant improvement in intensity above the background compared to the superimposed one (in blue), obtained in the conventional way of energy binning. A similar observation is noticeable when we compare the peak-to-total values (Tab. II.). There is a gain by a factor of two in the value for the 2-mm circle (top row) by including the polarization criterion. With the current investigation, we concluded that the polarization criterion improves the image quality in PET imaging only when the signal is relatively low above the background, also noted by McNamara et al. [18]. Experimental measurement of photon polarization requires a sensitive technique using the principle of Compton scattering [19]. A recent report [20] demonstrates the first measurement of polarization correlation with a full-scale tomograph, J-PET. Further advancement [21] using linear polarization of photons from positronium annihilations in studying the discrete symmetries is noteworthy.

Tab. II. Comparison of peak-to-total for energy and energy plus polarization--based filtering.

S. NO.	CIRCLE RADIUS (MM)	ENERGY BASED	ENERGY PLUS POLARIZATION
1	2	0.006	0.013
2	3	0.03	0.04
3	4	0.05	0.06
4	6	0.12	0.17
5	10	0.38	0.54

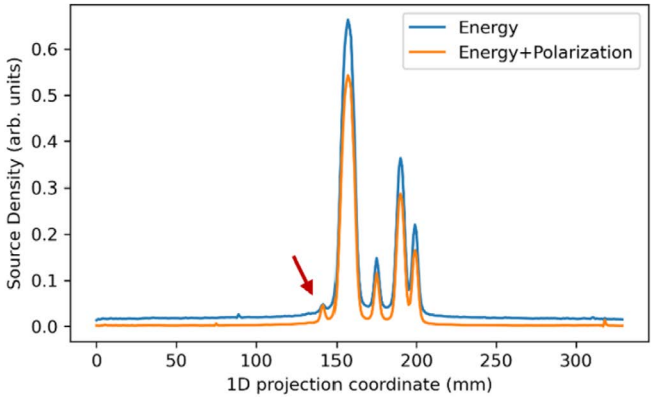

Fig. 8. Intensity plot for the reconstructed images for circles of different radii. Notably, the intensity increases with radius, and the circle of radius 1 mm is not visible. The arrow-marked peak corresponds to a circle of radius 2 mm showing a significant improvement for the orange.

CONCLUSIONS

We developed a mathematical analysis based on a simple geometrical construction to find the annihilation point in 2-D-PET imaging. Our approach utilized single scattering data, where one photon remained unscattered while the partner photon was scattered once within the phantom region. Our approach exclusively utilized the time-of-flight (TOF) information appropriate for organic scintillators like the plastic used in J-PET. Notably, PET systems employing organic scintillators are more cost-effective than conventional PET systems using inorganic scintillators. We reconstructed the image of a point source by identifying the loci of the annihilation point for many single-scattered events and then finding the overlapping region. The positioning of the intensity profile at its original location with a finite width confirmed the validity of our model. We believe

that the concepts presented here have opened up two research directions: firstly, the generalization of the model to 3-D; secondly, the experimental validation of our model with the J-PET data. We are pursuing both and facing challenges, especially in 3-D modelling with enhanced complexity.

The polarization-directional correlation of photons has been well--known for a long time. We have used the classical concept of orthogonal polarization of two annihilation photons to identify true events in PET imaging. Typically, an energy cut of 511 keV with an appropriate error, serves as the selection criterion with or without TOF. Applying the polarization condition further refines the selection and is expected to decrease noise from random coincidences. We have indeed observed a significant reduction in overall background at high event rates. Additionally, in some cases, we have noticed improved image quality, but more research is necessary to validate our findings.

CONFLICT OF INTEREST

Authors have declared no potential conflicts of interest.

REFERENCES

1. Zaidi H, Montandon M-L. Scatter compensation techniques in PET. PET Clin. 2014;2(2):219-34.
2. Bailey DL, Townsend DW, Valk PE, Maisey MN. Positron emission tomography. Basic Sciences. New York: Springer; 2005.
3. Conti M, Hong I, Michel C. Reconstruction of scattered and unscattered PET coincidences using TOF and energy information. Phys Med Biol. 2012;57(15):N307.
4. Hemmati H, Kamali-Asl A, Ay M, Ghafarian P. Compton scatter tomography in TOF-PET. Phys Med Biol. 2017;62(19):7641-58.
5. Ghosh S, Das P. Feasibility study of imaging with tissue-scattered triple-γ coincidence events in Compton-PET. JINST. 2022;17:P05040.
6. Yoshida E, Tashima H, Nagatsu K, Tsuji AB, Kamada K, Parodi K. Whole gamma imaging: a new concept of PET combined with Compton imaging. Phys Med Biol. 2020;65:125013.
7. Giovagnoli D, Bousse A, Beaupere N, Canot C, Cussonneau J-P, Diglio S, et al. A pseudo-TOF image reconstruction approach for three-gamma small animal imaging. IEEE Trans Rad Plas Med Sci. 2021:5(6):826-34.
8. Kolstein M, Chmeissani M. Using triple gamma coincidences with a pixelated semiconductor Compton-PET scanner: a simulation study. JINST. 2016;11:C01039.
9. Eppard E. Pre-therapeutic dosimetry employing scandium-44 for radiolabeling PSMA-617. In: Genadiev T, editors. Prostatectomy. London: IntechOpen; 2019. p. 1.
10. Ghosh S, Das P. Improvement of CNR in low-count PET scans using tissue-scattered data as initial estimate in non-TOF MLEM reconstruction. Biomed Phys Eng Express. 2023;9:035023.
11. Jan S, Santin G, Strul D, Staelens S, Assié K, Autret D, et al. GATE: a simulation toolkit for PET and SPECT. Phys Med Biol. 2004;49:4543.
12. Thielemans K, Tsoumpas C, Mustafovic S, Beisel T, Aguiar P, Dikaios N, et al. STIR: software for tomographic image reconstruction release 2. Phys Med Biol. 2012;57:867.
13. Moskal P, Dulski K, Chug N, Curceanu C, Czerwiński E, Dadgar M, et al. Positronium imaging with the novel multiphoton PET scanner. Sci Adv. 2021;7:eabh4394.
14. Moskal P, Rundel O, Alfs D, Bednarski T, Białas P, Czerwiński E, et al. Time resolution of the plastic scintillator strips with matrix photomultiplier readout for J-PET tomograph. Phys Med Biol. 2016;61(5):2025.
15. Moskal P, Baran J, Bass S, Choiński J, Chug N, Curceanu C, et al. Positronium image of the human brain in vivo. Sci Adv. 2024;10:eadp2840.
16. Kuncic Z, McNamara A, Wu K, Boardman D. Polarization enhanced X-ray imaging for biomedicine. Nucl Inst Meth Phys Res A. 2011;648:S208-10.
17. Allison J, Amako K, Apostolakis J, Arce P, Asai M. Recent developments in geant4. Nucl Inst Meth Phys Res A. 2016;835:186-225.
18. McNamara AL, Toghyani M, Gillam JE, Wu K, Kuncic Z. Towards optimal imaging with PET: An in-silico feasibility study. Phys Med Biol. 2014;59:7587-600.
19. Moskal P, Krawczyk N, Hiesmayr BC, Bała M, Curceanu C, Czerwiński E, et al. Feasibility studies of the polarization of photons beyond the optical wavelength regime łwith the J-PET detector. Eur Phys J C, 2018; 78: 970.
20. Moskal P, Kumar D, Sharma S, Beyene EY, Chug N, Coussat A, et al. Non-maximal entanglement of photons from positron-electron annihilation demonstrated using a novel plastic PET scanner. arXiv:2407.08574.
21. Moskal P, Czerwiński E, Raj J, Bass SD, Beyene EY, Chug N, et al. Discrete symmetries tested at 10−4 precision using linear polarization of photons from positronium annihilations. Nature Comm. 2024;15:78.